JOURNAL OF AIRCRAFT
Vol. 43, No. 4, July–August 2006

Numerical Simulation of Flare Safe Separation

Motti Adar,* Yuval Levy,† and Alon Gany‡
Technion—Israel Institute of Technology, 32000 Haifa, Israel

Numerical simulations are conducted to study the characteristics of a burning flare and their effects on the flare motion as it is released from an aircraft. Models concerning the shrinkage of the flare, mass addition to the flow, and heat addition to flow are devised and examined. The results show that the heat addition to the flow has the largest effect on the flare motion especially on its angular motion. The results also show that the angular motion has a small effect on the flare trajectory.

Introduction

PROTECTING aircraft from infrared (IR)-seeking air-to-air missiles involves dispersing IR decoys. An IR decoy, usually called a flare, is actually a rod made of a certain pyrotechnic material that burns in the air omitting IR radiation designed to capture the missile seeker and thus diverting the missile from the aircraft. An essential part of the process of certifying a flare to be carried on and released from an aircraft involves ensuring its safe separation from the parent aircraft (the aircraft from which it has been dispersed). Ensuring the safe separation of a flare from an aircraft is currently conducted mainly using flight tests because it cannot be conducted in wind tunnels caused by various obstacles. The first stems from the small size of a typical flare, approximately 20 to 30 mm in diameter, about two orders of magnitude smaller than the parent aircraft. Thus, when conducting a wind-tunnel test with a 20:1 scale model, the flare model diameter is about 1 to 2 mm. Such a small-sized model cannot be used in common wind-tunnel tests. Second, the flare is usually released in such directions that prohibits the use of a captive trajectory system (CTS) rig, even if the scale of the model allows it. And third, the flare is burning. Introducing a burning moving agent into a wind tunnel is an impractical task, thus prohibiting the use of wind-tunnel tests altogether.

The lack of tools for the prediction of flare motion promoted the development of robust (from a safe separation point of view) release mechanisms. Such mechanisms provide extended safety margins, thus avoiding issues of safe separation. The only feasible way to predict a flare motion relative to an aircraft prior to flight tests is by resorting to computational means. This paper utilizes computational-fluid-dynamics (CFD) analysis to study the characteristics of a burning flare. Physical models that represent special characteristics of a burning flare are devised and introduced into a CFD code. Numerical simulations of the flow about a flare as it is released underneath and above an F-16 aircraft wing are conducted to examine the effect of various parameters on the flare trajectory.

Technical Background

When releasing a store (a fuel tank, a bomb, a missile, a flare, etc.) from an aircraft, the first stage of the store motion is the separation stage. At this stage the store can hit the parent aircraft or nearby stores. Investigation of the store safe separation from the aircraft must be done before flight tests or any operational use can take place. There is a large number of parameters affecting the store behavior in the presence of an aircraft. Some of the parameters are listed as follows: 1) aircraft geometry, 2) presence of nearby stores, 3) Mach number, 4) dynamic pressure, 5) aircraft angle of attack and sideslip angle, 6) aircraft maneuver, 7) characteristics of the release mechanism, 8) position of the store on the aircraft, 9) release direction of the store, 10) ejection force/exit speed from a dispenser, 11) inertial properties of the store, and 12) aerodynamic configuration of the store.

The level of influence of each of the parameters is investigated as a part of the safe separation analysis as it changes from case to case. Flares have additional parameters that can influence their motion near the aircraft. The additional parameters that are related to the burning process of the flare are listed as follows: 1) size reduction of the flare, 2) heat transfer from the flare to the flow, 3) mass addition to the flow, 4) change in fluid composition in the vicinity of the flare, 5) ignition effect, and 6) ignition time. The effects of the preceding parameters on the flare motion during the separation phase are almost unknown because wind-tunnel tests cannot be performed to investigate these issues. A priori knowledge of the effects can provide important insight into the flare safe separation analysis.

This paper presents a study of the influence of the first three parameters on the motion of the flare during the separation phase. The physical models that are used to simulate the parameters are presented. Note, the burning process is viewed in this study as a source of energy (heat) and mass, and thus a detailed investigation of the burning process of the flare is not conducted. The reference pyrotechnic material parameters are taken from the typical material that composes flares, namely, magnesium Teflon® viton (MTV).

Size Reduction of the Flare

Because the flare is actually a solid propellant, the rate in which the flare is consumed can be described by the common empirical burning-rate formula

$$\dot{r} = a * p^n \tag{1}$$

where $\dot{r}$ is the burning rate, p is the pressure, and a and n are constants. Typical values of $a = 1.9$ and $n = 0.4$, where $\dot{r}$ is in mm/s and P is in atm, have been used in Eq. (1), yielding burning rates of a few mm/s in the relevant ambient conditions. Because the mass flow rate contributes only a negligible amount to the pressure, zero pressure gradient on the flare surface can be applied. As a result, the pressure on the flare is realized directly from the flow solution.

Heat Addition

It is assumed that the chemical reaction (combustion) and heat generation take place at the flare surface or very close to it. (Typically the chemical reaction of a solid propellant takes place within a very thin, less than 1 mm, layer above the burning surface.) Possible secondary reaction of the flare gases with the surrounding air far away from the surface is neglected. The heat transfer to the flow is then realized by applying an isothermic wall boundary where the wall temperature is the reaction temperature (assumed to be known). The heat-transfer rate to the flow is then obtained as a part of the solution of the flow equations.

Received 5 June 2005; revision received 24 October 2005; accepted for publication 25 October 2005.

*Graduate Student, Faculty of Aerospace Engineering.
†Senior Lecturer, Faculty of Aerospace Engineering.
‡Professor, Faculty of Aerospace Engineering.

Mass Addition

It is assumed that all of the mass of the flare consumed during the burning process becomes a gas. This assumption is more accurate as the temperature of the reaction rises. It is also assumed that the properties of the gas that is produced during the burning process are close enough to air so it can be addressed as air. Mass addition to the flow is calculated based on the empirical burn-rate formula [Eq. (1)]. Assuming a one-dimensional outgoing flow from the burning flare surface, the gas velocity perpendicular to the flare surface can be derived from the mass conservation, yielding

$$W = \dot{r} * \rho_{\text{flare}}/\rho_{\text{air}} \tag{2}$$

where W is the normal gas velocity component at the flare surface.

Geometry and Computational Mesh

The flow simulations conducted in this work are of the flow about a flare as it is released in the neighborhood of an F-16 aircraft wing. The flare geometry is modeled in the current work as a cylinder with two hemispheres at its ends. The flare is 20 cm long, and its diameter is 2.5 cm. The origin of the coordinate system is set at the root leading edge of the wing. The wing and flare coordinates are made dimensionless using the wing root as a reference length, and therefore all of the results presented herein are based on that reference length.

An efficient fashion to simulate the flow about moving geometries is the use of the overset grid method known as Chimera.[1] Using the Chimera approach, a separate mesh is generated for each component, and as a component is moving, or changing its orientation, the mesh is moving with it. For example, in the current case, the computational mesh is composed of two zones: one for the wing and the other for the flare (see Fig. 1). The wing mesh is stationary while the flare mesh moves together with the flare that, in turn, moves as a result of the gravitational and aerodynamic forces and moments exerted on it.

For nonintersecting solid components, the only complication introduced by using the Chimera method is because grid points of one mesh can lie within the solid boundaries of another mesh. This complication is resolved by removing these points from the computations. The process is termed as cutting "holes" through the computational domain (see Fig. 1). Flow variables at the edges of the holes are obtained through interpolations from the mesh in which they reside. Additional interpolations are required in order to obtain the proper boundary conditions at the outer boundaries of the meshes of each zone.

Numerical Scheme

The governing equations that are solved to simulate the flow about the flare are the Navier–Stokes or Euler equations. The dimensionless Navier–Stokes equations in body-conforming curvilinear coordinates can be written as

$$\frac{\partial \hat{\boldsymbol{Q}}}{\partial \tau} + \frac{\partial \hat{\boldsymbol{E}}}{\partial \xi} + \frac{\partial \hat{\boldsymbol{F}}}{\partial \eta} + \frac{\partial \hat{\boldsymbol{G}}}{\partial \zeta} = \frac{1}{Re}\left(\frac{\partial \hat{\boldsymbol{E}}_v}{\partial \xi} + \frac{\partial \hat{\boldsymbol{F}}_v}{\partial \eta} + \frac{\partial \hat{\boldsymbol{G}}_v}{\partial \zeta} \right) \tag{3}$$

where $\boldsymbol{Q}$ is the vector of conserved mass, momentum, and energy

$$\hat{\boldsymbol{Q}} = \frac{1}{J}\begin{bmatrix} \rho \\ \rho \bar{V} \\ e \end{bmatrix} \tag{4}$$

and J is the transformation Jacobian. The inviscid flux vectors are denoted by $\hat{\boldsymbol{E}}$, $\hat{\boldsymbol{F}}$, and $\hat{\boldsymbol{G}}$, while the viscous flux vectors are denoted by $\hat{\boldsymbol{E}}_v$, $\hat{\boldsymbol{F}}_v$, and $\hat{\boldsymbol{G}}_v$.

Time integration is conducted using the implicit algorithm of Beam and Warming[2,3] given by

$$\left(I + h\delta_\xi \hat{A} - hRe^{-1}\bar{\delta}_\xi \hat{A}_v^\xi\right)^n \qquad \left(I + h\delta_\eta \hat{B} - hRe^{-1}\bar{\delta}_\eta \hat{B}_v^\eta\right)^n$$

$$\left(I + h\delta_\zeta \hat{C} - hRe^{-1}\bar{\delta}_\zeta \hat{C}_v^\zeta\right)^n \qquad \Delta \hat{\boldsymbol{Q}}^n = \hat{\boldsymbol{R}}^n \tag{5}$$

where $\hat{\boldsymbol{R}}^n$ is

$$\hat{\boldsymbol{R}}^n = -\Delta t\left[\delta_\xi \hat{\boldsymbol{E}} + \delta_\eta \hat{\boldsymbol{F}} + \delta_\zeta \hat{\boldsymbol{G}} - Re^{-1}\left(\bar{\delta}_\xi \hat{\boldsymbol{E}}_v + \bar{\delta}_\eta \hat{\boldsymbol{F}}_v + \bar{\delta}_\zeta \hat{\boldsymbol{G}}_v\right)\right]^n \tag{6}$$

The Jacobian matrices $\hat{A}$, $\hat{B}$, and $\hat{C}$ are obtained through a Taylor-series expansion of the inviscid flux vectors. A similar Taylor-series expansion of the viscous flux vectors results in the viscous Jacobian matrices $\hat{A}_v^\xi$, $\hat{B}_v^\eta$, and $\hat{C}_v^\zeta$. The superscript n denotes evaluation at the nth time step where $t = n\Delta t$. The use of an implicit algorithm is necessary to provide high accuracy of the time-accurate simulation and to allow for a sufficiently large time step.

The computer code, called ZNSS,[4] is a flow solver that includes a suite of routines that handles the intergrid communications that are necessary for the Chimera overset grid approach. A number of modifications were introduced into the code in order to facilitate the flare motion simulation.

Dynamic Hole Size

As just mentioned, when using the Chimera method, holes are cut out of the various zones based on the location of solid boundaries. The method requires a sufficient overlap between zones to obtain good accuracy and robust transfer of information between zones. As the flare is moving, it might encounter regions where the wing mesh resolution is low, and therefore a hole in the size of the solid boundary of the flare might not provide a sufficient overlap. This can be overcome by using a virtual body face that is set at a larger shell of grid points than the original body face. This in turn can cause problems at areas where the wing mesh resolution is high because of expected large gradients or when the flare is close to the wing. Too large a hole can result in a loss of information transfer between zones or intersection between holes.

An algorithm for the dynamic setting of the hole size has been introduced to facilitate the motion of the flare through low resolution as well as high-resolution mesh regions. This is conducted according to the size of the cells of the surrounding mesh. The method involves calculating the size of the grid cells in the location of the flare and comparing this size to the known sizes of the flare grid shells and then choosing a grid shell that is larger than the local static grid cell size by a predefined factor. Calculating the size of the grid cells in the location of the flare is conducted using two methods. The first method is based on the cell volume V assuming a cubic-like cell

$$l = V^{\frac{1}{3}} \tag{7}$$

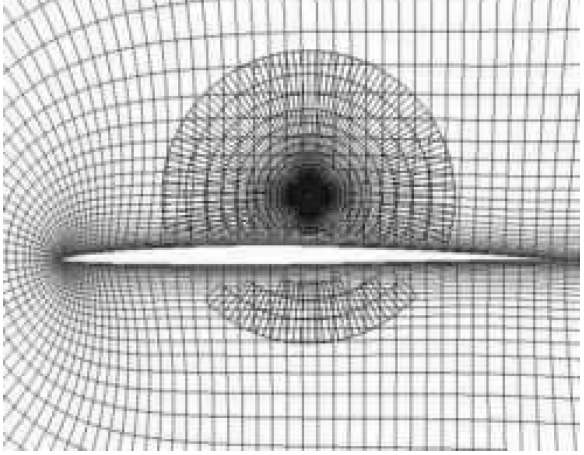

Fig. 1 Wing and flare grids with holes.

where l is the characteristic length. The second method calculates the maximum cell size by calculating cell size at every direction. For example, in the i coordinate direction

$$l_i = \{[X(i,j,k) - X(i+1,j,k)]^2 + [Y(i,j,k) - Y(i+1,j,k)]^2 + [Z(i,j,k) - Z(i+1,j,k)]^2\}^{\frac{1}{2}} \tag{8}$$

and then defining the local cell size as

$$l = \max\{l_i, l_j, l_k\} \tag{9}$$

Shrinkage of the Flare Mesh

The burning process of the flare causes its size to shrink, and therefore a shrinkage model for the flare computational mesh is introduced. The shrinkage model is based on the assumption that at each point shrinkage is always perpendicular to the surface of the flare. This assumption is consistent with the theory of solid-propellant combustion. The process of shrinking the flare computational mesh involves calculating the shrinkage size at each grid point on the surface of the flare using Eq. (1). Then, the new location of every point on the flare surface is calculated using the shrinkage direction (a vector perpendicular to the surface at the grid point, indicating into the body) and the shrinkage size. A parametric line is defined for each radial grid line, and the points on that grid line are moved toward the flare along the parametric line. The movement size of each point is equal to the local shrinkage size. Two types of shrinkage model have been applied: variable shrinkage and uniform shrinkage. Variable shrinkage means a varying shrinkage size, based on the local burn rate, for each surface grid point, whereas uniform shrinkage means that an average shrinkage size is calculated and applied at all surface grid points.

Flare Equations of Motion

Motion calculation of the flare is conducted using the rigid-body six-degrees-of-freedom (DOF) equations. The six-DOF routine is incorporated into the flow solver in such a way that at every time step the motion of the flare is calculated. The process of simulating the flare motion is composed of the following steps. First, the flowfield is calculated, and the aerodynamic forces and moments, in inertial coordinate system, are obtained through integration. Then, the incremental motion is calculated by solving the six-DOF equations. And finally, the flare is translated and rotated to the new position and attitude.

The six-DOF model that was developed for the current work contains special features that are necessary for the flare simulation. The model varies from the classical model by the following two main features. First, the model was developed for bodies whose mass and inertia moments are a function of time. And second, the model solves the equation of linear motion in inertial space while it solves the equation of angular motion in body coordinates. The aerodynamic coefficients are given in the inertial coordinate system, and therefore it is natural to solve the equation of linear motion in the inertial space. However, a similar solution of the equation of angular motion introduces off-diagonal elements in the inertia matrix. Therefore, the equation of angular motion is solved in a body coordinate system.

To reduce the complexity level of the six-DOF model, the following two assumptions were made. The motion of the flare is calculated only for releases from an aircraft flying at a leveled flight. And, the Euler explicit integration method is used to advance the solution. Because the time step is very small (about 2×10^{-6}) and the overall simulation time is small also (about 0.1 to 0.2 s), it is assumed that the numerical errors are also small. The equation of linear motion is based on the second law of Newton, namely,

$$\sum \boldsymbol{F} = \frac{\mathrm{d}[m(t)\boldsymbol{V}]}{\mathrm{d}t} \tag{10}$$

or in the current case

$$\sum \boldsymbol{F} = \boldsymbol{V}\frac{\mathrm{d}m(t)}{\mathrm{d}t} + m(t)\frac{\mathrm{d}\boldsymbol{V}}{\mathrm{d}t} \tag{11}$$

where $m(t)$ is the instantaneous flare mass. The first term in Eq. (11) is zero when the shrinkage of the flare is uniform and can be neglected even when variable shrinkage is employed, arriving at

$$\sum \boldsymbol{F} = m(t)\,\frac{\mathrm{d}\boldsymbol{V}}{\mathrm{d}t} \tag{12}$$

Applying forward differences, Eq. (12) becomes

$$\boldsymbol{V}^{n+1} = \begin{bmatrix} u^{n+1} \\ v^{n+1} \\ w^{n+1} \end{bmatrix} = \boldsymbol{V}^n + \Delta t \begin{bmatrix} \dfrac{q_\infty S C_X^{n+1}}{m^{n+1}} \\ \dfrac{q_\infty S C_Y^{n+1}}{m^{n+1}} \\ \dfrac{\left(q_\infty S C_Z^{n+1} - m^{n+1} g\right)}{m^{n+1}} \end{bmatrix} \tag{13}$$

where q_∞ is the dynamic pressure, S is the reference area, and C_X, C_Y, and C_Z are the force coefficients. The incremental motion of the center of gravity of the flare is then calculated using an average velocity as follows:

$$\begin{bmatrix} \Delta_x \\ \Delta_y \\ \Delta_z \end{bmatrix} = \frac{\Delta t}{2} \begin{bmatrix} u^{n+1} + u^n \\ v^{n+1} + v^n \\ w^{n+1} + w^n \end{bmatrix} \tag{14}$$

The flare angular motion is evaluated using the equation of angular motion in body coordinates. In an inertial coordinate system, the equation is given by

$$\sum \boldsymbol{M}' = \frac{\mathrm{d}\boldsymbol{H}'}{\mathrm{d}t} \tag{15}$$

where $\boldsymbol{M}'$ and $\boldsymbol{H}'$ represent the moment vector and the angular momentum vector, respectively. In body coordinates, the equation takes the form:

$$\sum \boldsymbol{M} = \frac{\mathrm{d}\boldsymbol{H}}{\mathrm{d}t} + \boldsymbol{\Omega} \times \boldsymbol{H} \tag{16}$$

where $\boldsymbol{\Omega}$ is the angular velocity vector whose components are commonly represented as

$$\boldsymbol{\Omega} = \begin{bmatrix} p \\ q \\ r \end{bmatrix} \tag{17}$$

The angular momentum $\boldsymbol{H}$ is given by

$$\boldsymbol{H} = I \cdot \boldsymbol{\Omega} \tag{18}$$

where I is the inertia matrix.

Following a similar formulation as for the equation of linear motion, the following relation for the angular acceleration is obtained:

$$\begin{bmatrix} \dot{p} \\ \dot{q} \\ \dot{r} \end{bmatrix} = \begin{bmatrix} \dfrac{M_x^{n+1} - q^n r^n \left(I_z^{n+1} - I_y^{n+1}\right)}{I_x^{n+1}} \\ \dfrac{M_y^{n+1} - p^n r^n \left(I_x^{n+1} - I_z^{n+1}\right)}{I_y^{n+1}} \\ \dfrac{M_z^{n+1} - p^n q^n \left(I_y^{n+1} - I_x^{n+1}\right)}{I_z^{n+1}} \end{bmatrix} \tag{19}$$

The new Euler angles of the body are then calculated in the same fashion as the new center-of-gravity location is calculated. Once the new location and orientation are known, the flare mesh is transformed to its new state.

Table 1 Starting conditions

Condition	Mach	α	X_0	Y_0	Z_0	θ_0	ϕ_0	ψ_0	U_0	V_0	W_0	$\dot{\theta}_0$	$\dot{\phi}_0$	$\dot{\psi}_0$
1	0.8	5	0.7	0.3	−0.05	0	0	0	−20	0	0	0	0	0
2	0.6	5	0.6	0.27	0.1	0	0	−90	0	30	0	0	0	0

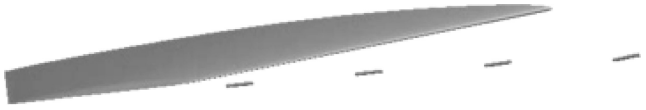

Fig. 2 Flare motion underneath an F-16 aircraft wing.

Fig. 3 Flare motion above an F-16 aircraft wing.

Results

Prior to embarking on the numerical analysis, several numerical tests have been conducted. These tests included a grid-resolution study, a time-step sensitivity study, and a numerical scheme validation study. The grid-resolution study showed that the results were grid independent. Following the grid-resolution study, the time step was cut by half, and the results, including forces moments and trajectories, were compared. The results showed no difference whatsoever. For complete details of the grid resolution and time-step studies, see Ref. 5. The numerical scheme validation included flow solver validation, six-degrees-of-freedom motion calculation validation, and the Chimera method validation. The results were favorably compared against experimental data. Complete details of the numerical scheme validation can be found in Ref. 6.

Following the just-mentioned validation, numerical simulations of the flare motion from two starting conditions were conducted and presented (see Table 1). The first starting condition corresponds to a flare moving forward, underneath an F-16 aircraft wing (see Fig. 2), whereas the second starting condition corresponds to a flare moving across the streamwise flow, above the same wing (see Fig. 3). The first four numerical simulations in the first starting condition were conducted using an inviscid flow assumption because it was assumed that the flow about the flare, in this case, will have none or very small viscous characteristics. Because it was found that the separation at the aft part of the flare has a profound effect on the motion of the flare, three additional simulations were conducted using a viscous, turbulent flow assumption. The simulations of the first starting condition using the inviscid flow assumption are presented because they provide a valuable insight. All of the simulations concerning the second starting condition were conducted using a turbulent flow assumption for the flow about the flare and an inviscid flow assumption for the flow about the wing. An inviscid flow assumption can be used for the wing because the wing is placed at a small angle of attack and because the influence of the flare on the flow about the wing is localized and small. The Baldwin–Lomax turbulence model[7] was used to model the turbulence.

Seven different types of flare simulation were considered for the first starting condition where flare characteristics are varied systematically to allow for a parametric investigation (see Table 2). In the first type, it is assumed that the flare is not burning, and therefore neither heat nor mass is added to the flow, and the flare geometry remains unchanged. This type of simulation is heretoforth referred to as "solid flare." The second type is conducted under the assumption that the consumption of the flare influences the flare geometry only, that is, the flare shrinks. This type of simulation is conducted to isolate the effect of the flare shrinkage on its motion. The third simulation type is of a shrinking flare while mass (the mass of the flare that is consumed as a result of the burning process) is added to the flow as gas. This type of simulation isolates the effect of mass addition to the flow. The fourth simulation type, termed here a "hot flare," treats the flare as a heat source without any change to its shape and without mass addition. The heat addition to the flow is modeled by applying an isothermal wall boundary on the flare surface. The surface temperature in this case is 1800 K, approximately the lower limit of the MTV reaction temperature.[8] All of these runs were conducted using the inviscid flow assumption. The fifth simulation type incorporates all three described models, namely, it is a hot flare simulation with mass addition to the flow and shrinkage of the flare. The wall temperature is set to 1800 K in this case as well. This is the most realistic flare simulation conducted under the first starting condition. The sixth and seventh simulations are similar to the first and the fourth when the difference is that the solution about the flare in these simulations and in the fifth simulation is a viscous solution.

Table 2 Simulation types; first starting condition

Simulation type	Shrinkage	Mass additions	Heat addition (surface temperature)	Solution
1	No	No	No	Inviscid
2	Yes	No	No	Inviscid
3	Yes	Yes	No	Inviscid
4	No	No	Yes (1800 K)	Inviscid
5	Yes	Yes	Yes (1800 K)	Viscous
6	No	No	No	Viscous
7	No	No	Yes (1800 K)	Viscous

Table 3 Simulation types; second starting condition

Simulation type	Shrinkage (type)	Mass additions	Heat addition (surface temperature)
1	Yes (uniform)	Yes	No
2	No	No	Yes (1800 K)
3	Yes (uniform)	Yes	Yes (1800 K)
4	Yes (variable)	Yes	Yes (1800 K)
5	No	No	Yes (3000 K)

A comparison of the motion of the flare in six degrees of freedom using the inviscid solution is presented in Fig. 4. Motion comparison of the viscous solutions is presented in Fig. 5. A close examination of Figs. 4 and 5 shows that mass addition and changes to the flare geometry (the shrinkage of the flare) have a negligible effect on the flare motion, whereas heat addition has a sizable effect on the flare motion. The results show that heat addition to the flow causes the flare to have a more restrained angular motion. It also causes a slightly larger lateral motion.

Five simulation types were considered for the second starting condition. In light of the just-presented results for the first starting condition, all but one type included heat addition. To examine the effect of high reaction temperature on the flare motion, one of the cases included a surface temperature of 3000 K, which is approximately the upper limit of the MTV compositions reaction temperature.[8] In addition, one case of variable flare shrinkage has been conducted. All five simulation types are listed in Table 3.

Motion of the flare in six degrees of freedom is presented in Fig. 6. Figure 7 presents comparisons of flare motion in six degrees of freedom between uniform and variable shrinkage. The results show that as the temperature of the reaction rises the effect of the heat addition on the flare motion is more noticeable. This result is consistent with that obtained from the first starting condition. Similarly, it can be

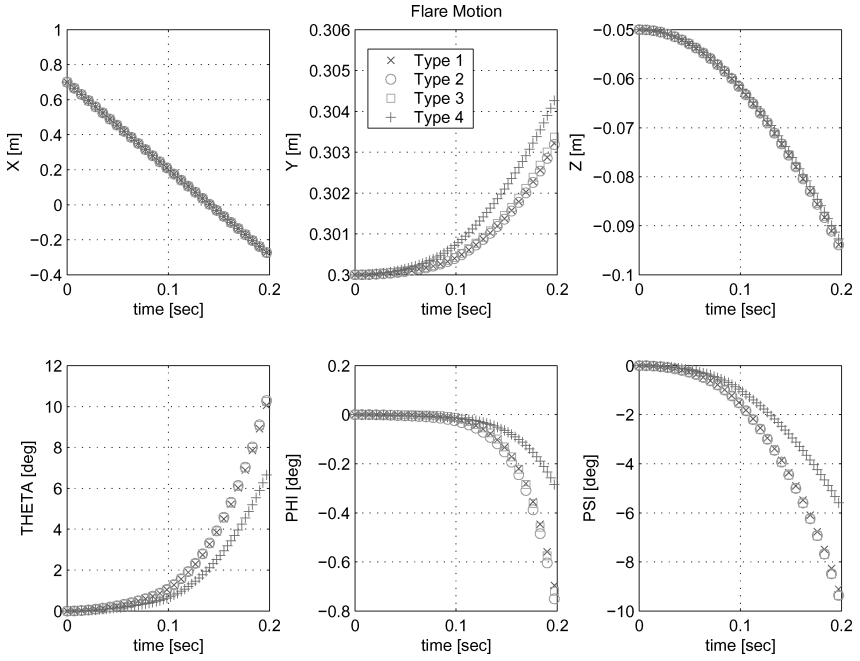

Fig. 4 Flare position and attitude comparison for the first starting condition; inviscid flow assumption.

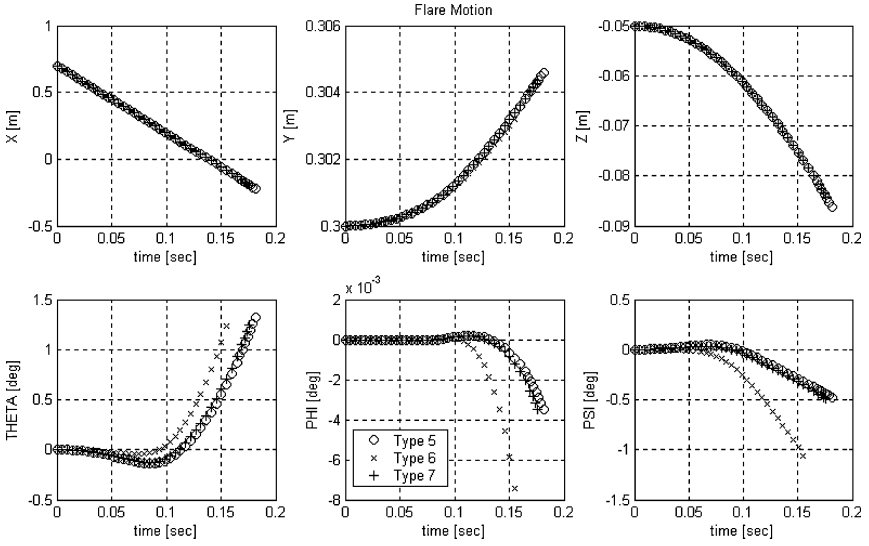

Fig. 5 Flare position and attitude comparison for the first starting condition; viscous flow assumption.

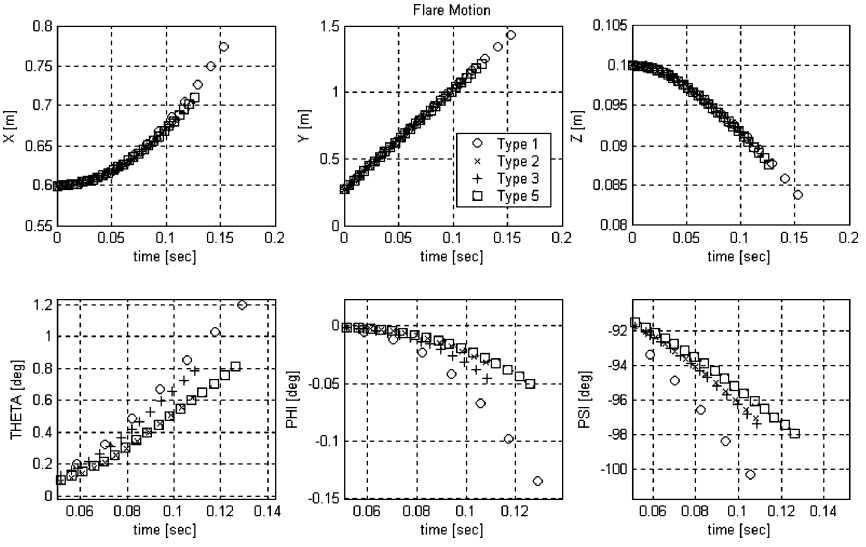

Fig. 6 Comparison of flare motion for the second starting condition.

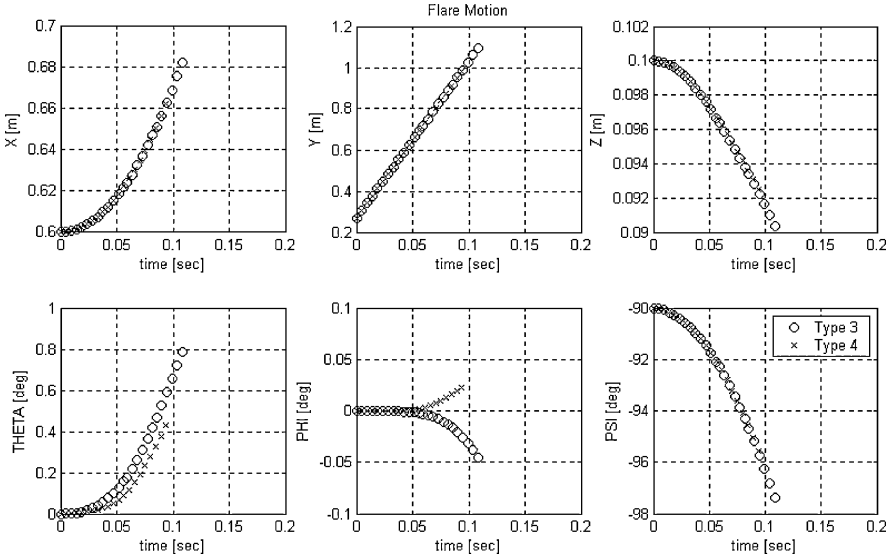

Fig. 7 Comparison of flare motion, uniform vs variable shrinkage; second starting condition.

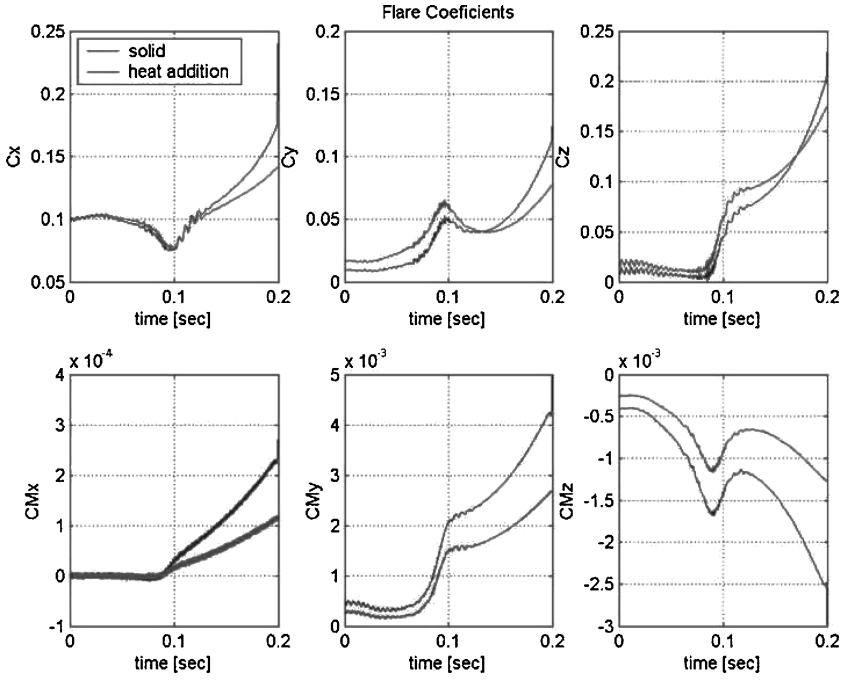

Fig. 8 Comparison of the flare aerodynamic coefficients for the first starting condition; inviscid flow assumption.

seen that heat addition causes the flare to have a more restrained angular motion. In addition, the following observations can be made. The first is that when heat transfer is present mass addition to the flow has an effect on flare motion; this effect is rather small, and mass addition to the flow can be neglected. The second is that the variable shrinkage model affects only slightly the roll motion of the flare.

Discussion

The results presented in the preceding section show that the heat addition has a similar effect on the flare motion for both starting conditions considered in this work. Specifically, the heat addition causes a reduction in the pitch and yaw rates of the motion to make the angular motion more restrained. To understand this phenomenon, the aerodynamic coefficients of the flare as it moves away from the first starting condition are examined.

A comparison of the aerodynamic coefficients of the flare with and without heat addition for the first starting condition (Figs. 8 and 9) reveals two main phenomena. The first is the effect of the wing on the flare aerodynamic coefficients. The aerodynamic coefficients change dramatically as the flare passes the wing leading edge; this occurs around $t = 0.1$ s. The second is the effect of the heat addition. Although heat addition has only a minor effect on the forces, it has a significant and a consistent effect on the aerodynamic moments about the flare (in particular, the yawing and pitching moments). The net result of the heat addition is a reduction of the yawing and pitching moments and, in turn, a more restrained angular motion.

Figure 10 shows the pressure coefficient distribution above and below the flare with and without heat addition. The pressure coefficient variation reflects the pitching moment on the flare. A close examination of the pressure coefficient distribution shows that the differences between C_p above and below the flare in the

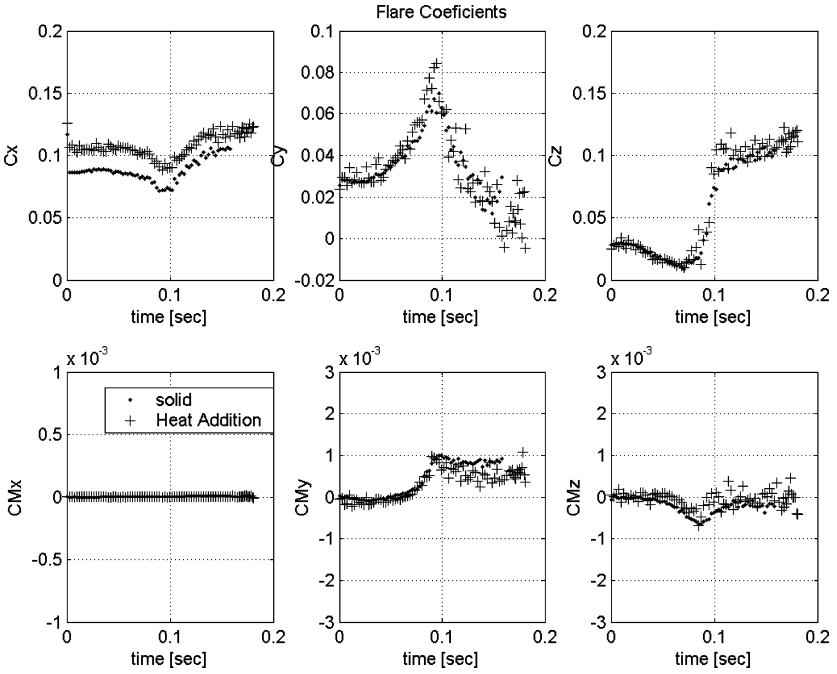

Fig. 9 Comparison of the flare aerodynamic coefficients for the first starting condition; viscous flow assumption.

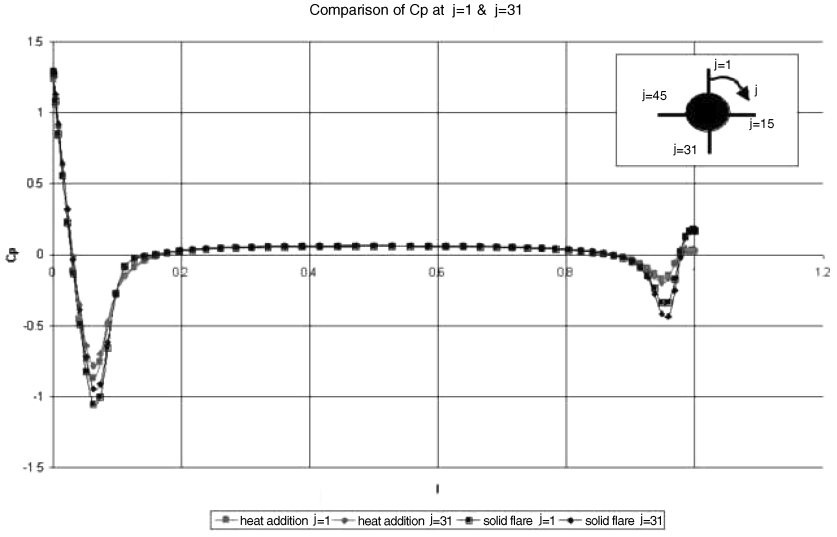

Fig. 10 Comparison of pressure coefficient above ($j = 1$) and below ($j = 31$) the flare; first starting condition.

aft section practically vanish when heat is added. This, in turn, results in a smaller pitching moment. (The same phenomenon is present for the yawing moment.) The uniform pressure when heat addition is present is a result of the large and uniform separation, as can be seen in Fig. 11. The large and uniform separation is, in itself, a direct result of the increased flow velocity and decreased pressure at the aft section of the flare; both occur as a result of the heat addition to the flow. Note, the results shown in Fig. 11 are obtained from inviscid flow simulations. The flow separation prompted the decision to repeat the calculations using a viscous flow assumption. Nevertheless, the results presented in the figure illustrate the effect of heat addition. The flow contains massive separation even with an inviscid flow assumption. The same behavior is exhibited by the viscous flow simulations.

The same phenomenon is present for the second starting condition. The uniform pressure distribution when heat addition is present (which can be seen in Figs. 12 and 13) reflects the large and uniform separation (Fig. 14). Hence, the uniform separation is the cause for the uniform pressure distribution, which leads to the reduced moments on the flare (see Fig. 15).

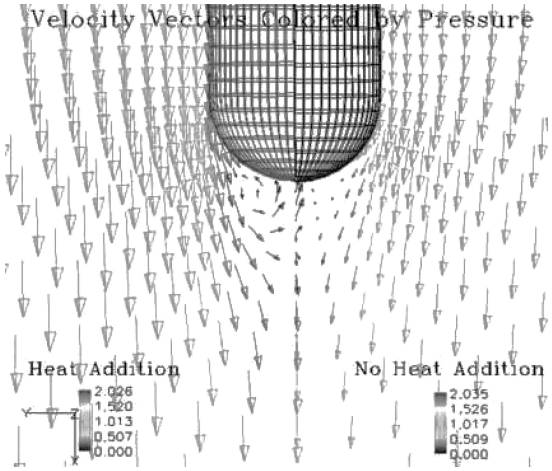

Fig. 11 Comparison of flow separation behind the flare (velocity vector field represented by arrow colored by normalized pressure), first starting condition.

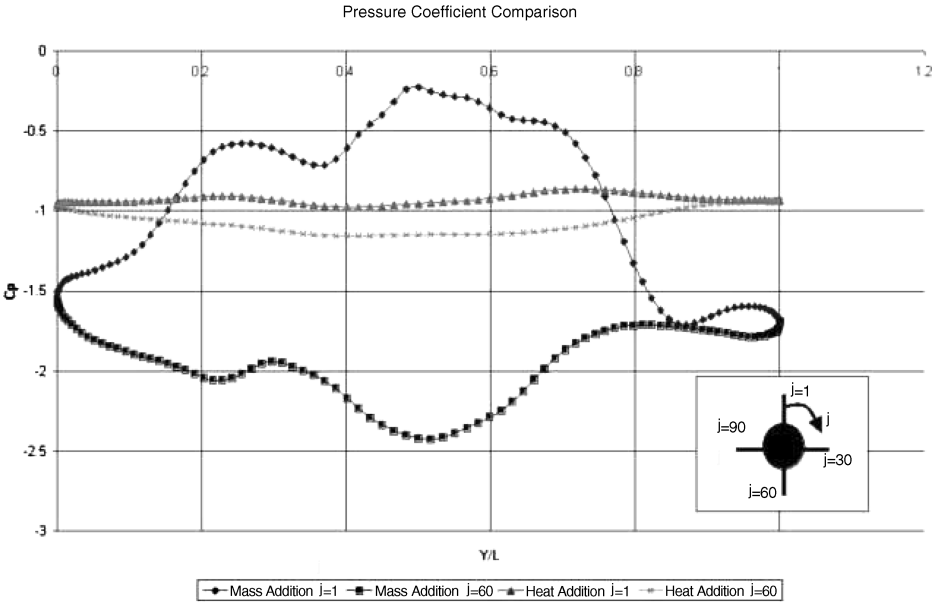

Fig. 12 Comparison of pressure coefficient above ($j = 1$) and below ($j = 60$) the flare; second starting condition.

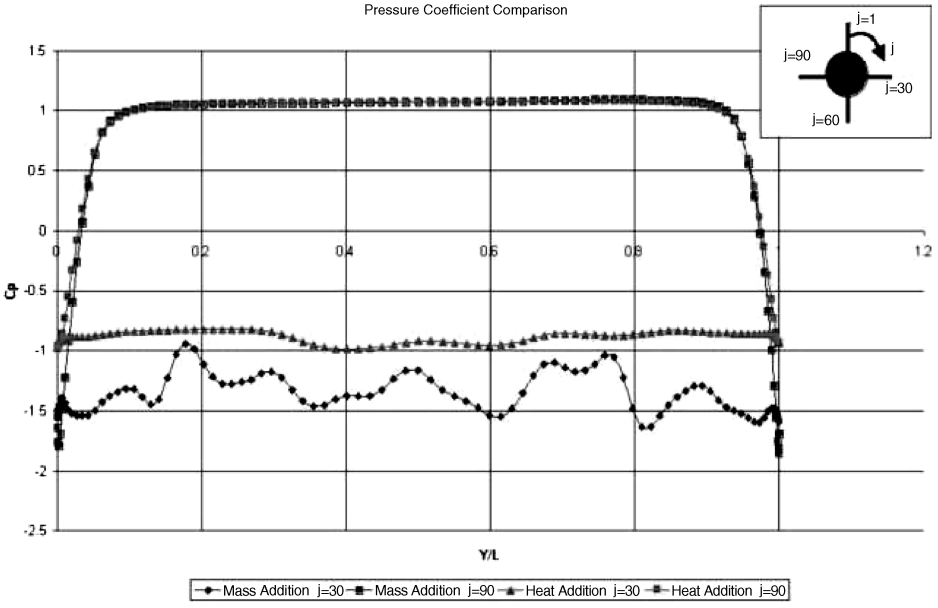

Fig. 13 Comparison of pressure coefficient in front ($j = 30$) and aft ($j = 90$) of the flare; second starting condition.

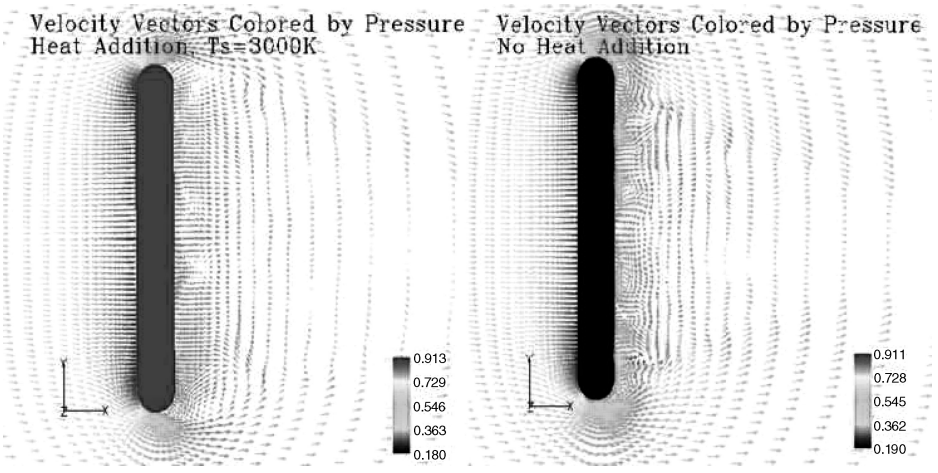

Fig. 14 Comparison of flow separation behind the flare; second starting condition.

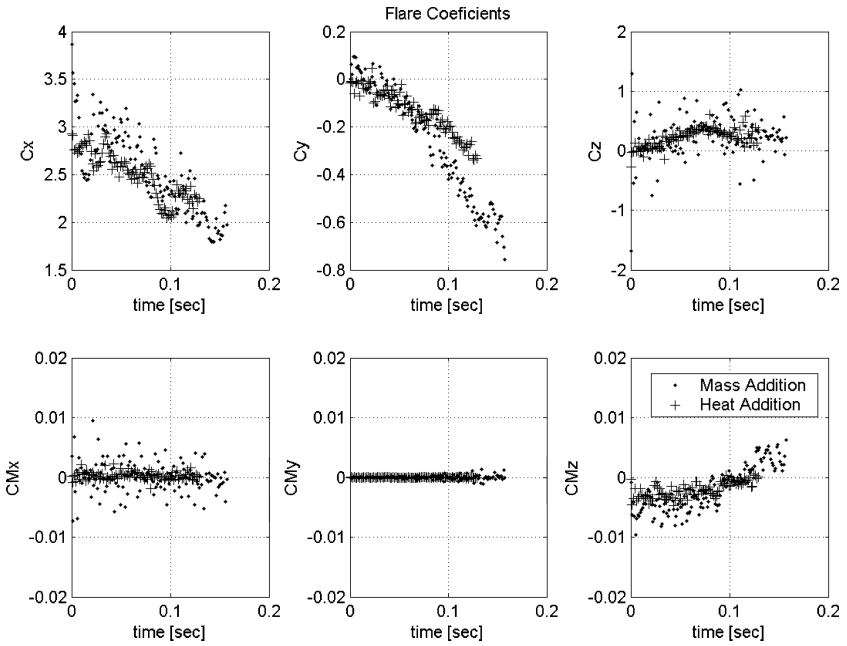

Fig. 15 Comparison of aerodynamic coefficients with and without heat addition; second starting condition.

Conclusions

The results presented in this paper allow the assessment of the effects of the special characteristics of a flare on its motion in the vicinity of an aircraft. The three characteristics considered in this work—shrinkage, mass addition, and heat addition—are a direct result of the burning process of the flare.

The results for both starting conditions show that there is a negligible effect of the shrinkage and mass addition on the flare motion. However, heat addition has a sizable effect on the flare motion, especially on the angular motion. The effect of the heat transfer mainly reduces the angular motion of the flare in respect to cases where heat transfer is not present. This effect is noticeable for both starting conditions and in all of the angular directions, that is, pitch, yaw, and roll. The cause for the reduced angular motion when heat addition is present is the large and uniform separation of the flow, especially around the aft part of the flare. Closer inspection of the results shows that when heat transfer is present mass addition also has an influence on the flare motion. Because this influence is small, the effect of the mass addition on the flare motion can be considered negligible.

An interesting effect is the effect of the type of shrinkage method. As just mentioned, two types of shrinkage methods were considered: uniform and variable shrinkage. One can see from the comparison in Fig. 7 that the shrinkage method only affects the roll motion of the flare. It can be seen that when one changes the type of the shrinkage method the direction of the roll motion changes. Because roll motion has no effect on the flare trajectory nor does it have any effect on the miss distance, it is concluded that shrinkage, variable or uniform, can be neglected in most cases. Consequently, numerical and coding efforts can be reduced even in cases where simulating heat transfer is needed. In such cases, simulating the heat transfer (and maybe even the mass addition) without simulating the shrinkage should be considered.

Another important observation is the fact that a difference in angular motion results in a negligible effect on the flare trajectory. Therefore, when the expected miss distance is large or it is known that angular motion is of no specific importance or there is no influence to the physical effect of the heat addition (that is, the acceleration of the flow about the flare), one could use a solid flare simulation.

Acknowledgment

The authors would like to thank Gil Iosilevskii of the Faculty of Aerospace Engineering at the Technion for hours of fruitful discussions concerning the six-degrees-of-freedom model and to Gabi Avital of the Israeli Military Industry for assisting in finding information regarding flares.

References

[1]Benek, J. A., Buning, P. G., and Steger, J. L., "A 3-d Chimera Grid Embedding Technique," AIAA Paper 85-1523, July 1985.

[2]Beam, R. M., and Warming, R. F., "An Implicit Finite-Difference Algorithm for Hyperbolic Systems in Conservation Law Form," *Journal of Computational Physics*, Vol. 22, Sept. 1976, pp. 88–110.

[3]Beam, R. M., and Warming, R. F., "An Implicit Factored Scheme for the Compressible Navier–Stokes Equations," *AIAA Journal*, Vol. 16, No. 4, 1978, pp. 393–402.

[4]Levy, Y., "Numerical Simulation of Dynamically Deforming Aircraft Configurations Using Overset Grids," *Journal of Aircraft*, Vol. 38, No. 2, 2001, pp. 349–354.

[5]Adar, M., "Numerical Study of Flare Separation," Master's Thesis, Aerospace Dept., Technion—Israel Institute of Technology, Haifa, Israel, Feb. 2005.

[6]Adar, M., and Levy, Y., "Preliminary Validation of a Chimera Based Flow Solver for Store Separation Simulation," *Proceedings of the 45th Israel Annual Conference on Aerospace Sciences*, Feb. 2005.

[7]Baldwin, B. S., and Lomax, H., "Thin Layer Approximation and Algebraic Model for Separated Turbulent Flows," AIAA Paper 78-257, Jan. 1978.

[8]Griffiths, T. T., and de Yong, L. V., "The Use of Equilibrium and Kinetic Computer Programs to Study the Combustion of mtv Formulations," *Proceedings of the 19th International Pyrotechnics Seminar*, International Pyrotechnic Society, Christchurch, New Zealand, Feb. 1994, pp. 556–572.